Journal of Alloys and Compounds 618 (2015) 635–642

Contents lists available at ScienceDirect

Journal of Alloys and Compounds

journal homepage: www.elsevier.com/locate/jalcom

Structural, hyperfine and Raman properties of RE_2FeSbO_7 compounds

G. Berndt [a], K.L. Silva [a], F.F. Ivashita [a], A. Paesano Jr. [a,*], M.C. Blanco [b], E.V.P. Miner [b], R.E. Carbonio [b], S.M. Dantas [c], A.P. Ayala [c], O. Isnard [d]

[a] Departamento de Física, UEM, Av. Colombo, 5790, 87.020-900 Maringá, PR, Brazil
[b] INFIQC-CONICET, Departamento de Físico Química, Facultad de Ciencias Quimicas, Universidad Nacional de Córdoba, Argentina
[c] Departamento de Física, Universidade Federal do Ceará, Brazil
[d] Institut Néel CNRS/Université de Grenoble, France

ARTICLE INFO

Article history:
Received 7 March 2014
Received in revised form 5 August 2014
Accepted 7 August 2014
Available online 3 September 2014

Keywords:
Pyrochlore
Site disorder
Rietveld analysis
Raman bands
Mössbauer spectroscopy

ABSTRACT

Pyrochlores of the RE_2FeSbO_7 type were synthesized by ball-milling followed by annealing in free atmosphere at high temperatures. The samples prepared were characterized by X-ray diffraction, Raman spectroscopy and ^{57}Fe Mössbauer spectroscopy, at room temperature. The results showed that RE_2FeSbO_7 compounds have a cubic structure, i.e., *Fd*-3*m* (#227) space group, and that a site disorder takes place for the RE's of larger ionic radii. Lattice parameters, Raman bands and quadrupole splittings were shown to depend correlatedly on the RE ionic radius. This behavior is discussed in terms of the pyrochlore crystallographic structure.

1. Introduction

Pyrochlores are oxides with the ideal formula $A_2B_2O_7$, where A and B are in general large trivalent and small tetravalent cations, respectively. These compounds are predominantly cubic and ionic in nature, and represent a family of phases which are isostructural to the mineral pyrochlore $(NaCa)(NbTa)O_6(F, OH)$. The $A_2B_2O_7$ compounds exhibit a wide variety of interesting physical properties, the geometric magnetic frustration (GMF) being the most striking [1–3]. Pyrochlores are extensively used in practical applications, such as switching elements, thermistors, thick-film resistors, materials for screen printing and nuclear waste immobilization.

For most of the pyrochlores studied in the phenomenological scenario of magnetic frustration, A is a magnetic rare-earth cation (RE^{3+}) and B is a non-magnetic cation, usually a transition tetravalent cation, M^{4+} (e.g., Ti^{4+}, Sn^{4+}, Zr^{4+}). In these cases, the only magnetic sublattice is the one formed by the rare-earth cations, which form a structure of sharing corners tetrahedra. In a few cases, $RE_2M_2O_7$ pyrochlores were prepared with transition cations which could, plausibly, have magnetic moments [4,5].

However, it is possible to synthesize these compounds with more than one chemical species, either at the site A or at the site B, provided that the ionic radius and charge neutrality criteria are satisfied [6]. Looking especially for what is the role of a magnetic transition cation (e.g., Mn^{4+} or Fe^{3+}) at sites B, i.e., regarding to crystallographic features and to the GMF, we have recently investigated the RE_2FeTaO_7 system [7]. The presence of iron (usually trivalent) offers the possibility of examine these systems by Mössbauer spectroscopy though, at principle, it requires a pentavalent partner cation (i.e., Ta^{5+}) sharing the same site (B), to match the electronic balance. In spite of being compounds iso-stoichiometric to the "classic" ternary pyrochlores, it was observed, among other properties, that these systems crystallize with the rhombohedral symmetry (*R*-3*m*). A couple of RE_2FeSbO_7 systems (RE = Gd, Y) was earlier surveyed [8–10] revealing that, differently of the RE_2FeTaO_7 compounds, show the same cubic structure of the ternary pyrochlores (*Fd*-3*m*), as reported in previous X-ray diffraction ordinary studies [11].

In this paper, we report results on the structural properties of RE_2FeSbO_7 pyrochlores, extending our investigation to most of the RE. A more complete structural description of the RE_2FeSbO_7 compounds is presented, by combining the Rietveld method for refining diffractograms – not earlier applied – with Mössbauer spectroscopy. The phonon spectra for this pseudo-ternary system were also obtained by Raman spectroscopy and the results discussed on basis of the crystallographic aspects of these sub-family of pyrochlores.

* Corresponding author. Tel./fax: +55 44 32634623.
E-mail address: paesano@wnet.com.br (A. Paesano Jr.).

http://dx.doi.org/10.1016/j.jallcom.2014.08.068
0925-8388/

2. Experimental details

The RE_2FeSbO_7 (with RE = Pr, Nd, Sm, Eu, Gd, Tb, Dy, Y, Ho, Er, Yb) samples were prepared, first, by ball-milling a blend of RE_2O_3, α-Fe_2O_3 and Sb_2O_5 powders (all 99.9% pure), mixed in a 2:1:1 M ratio. The precursors were milled for 3 h in a vial of alumina (80 ml) with zirconia rods, under argon atmosphere, using a planetary ball mill. The ball-to-powder mass ratio was 20:1 and the rotation speed was 300 rpm. After milling, the powders were annealed in free atmosphere for 6 h, at temperatures between 1200 °C and 1400 °C. The samples were cooled to room temperature by turning off the furnace. The same synthesis procedure was repeated for some selected samples, aiming to check the reproducibility of the preparation method, regarding the properties of interest. No significant loss of mass was ever detected for the prepared samples, respectively to the initial mass of the precursors.

The compounds were structurally characterized by powder X-ray diffraction (PXRD), Mössbauer spectroscopy (MS) and Raman spectroscopy (RS). The X-ray diffractograms were measured at room temperature, using the Cu Kα radiation (λ = 1.5418 Å), in a conventional diffractometer, in the θ–2θ Bragg–Brentano geometry. The 2θ range was from 5° up to 150°, with increments of 0.02° and a counting time of 6 s per step. The FULLPROF program [12] was applied to refine the crystal structure by the Rietveld method. A pseudo-Voigt shape function was used to fit the experimental data. The data refined were atomic positions, lattice parameters, peak shape, isotropic thermal parameters, and occupation factors.

The Raman spectra were recorded with a triple spectrometer, with a liquid-nitrogen-cooled charge-coupled device (CCD). The slits were set to give a spectral resolution better than 2 cm^{-1}. The spectra were excited with the 532 nm line of diode pumped solid state laser, operating at 30 mW. These spectra were corrected by the Bose–Einstein occupation factor for Stokes processes $[n(\omega)+1]$, where $n(\omega) = 1/\exp(h\omega/k_BT)$.

Mössbauer spectra were taken at RT, from a constant acceleration spectrometer with a ^{57}Co(Rh) source, using absorbers with nearly 67 mg/cm^2. The numerical fits were done considering a Lorentzian line shape and applying the criterion of the minimum chi-squared.

3. Results and discussion

3.1. Powder X-ray diffraction

Some representative refined diffractograms for the RE_2FeSbO_7 pyrochlores are shown in Fig. 1. These compounds – in fact, all RE_2FeSbO_7 samples – showed the structure of the $A_2B_2O_7$ cubic pyrochlores (see Fig. 2), i.e., *Fd*–3*m* (#227) space group, with cell parameter around 10 Å. Therefore, this is different from what happens when tantalum is the partner of iron (i.e., RE_2FeTaO_7 pyrochlore), in which case the lattice is rhombohedral [7].

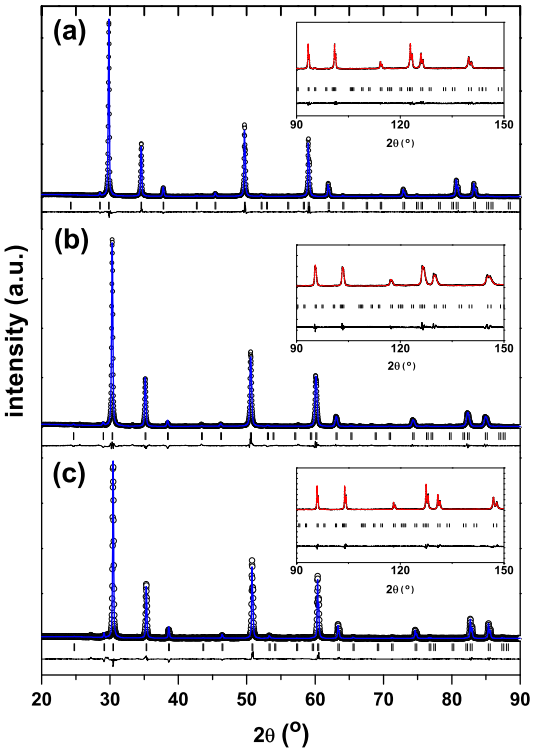

Fig. 1. Refined diffractograms for the Nd_2FeSbO_7 (a), Sm_2FeSbO_7 (b) and Yb_2FeSbO_7 (c) samples.

In general, for the RE_2FeSbO_7 pyrochlores, all cations occupy special positions – i.e., there is one Wyckoff site for the RE cations (site 16*c*) and one for the transitions cations (site 16*d*). Oxygen also occupies one special position (8*a*) and one site (site 48*f*) for which there is a variable positional parameter, *x*. Like for the ternary compounds, the RE cations are 8-coordinated, whereas Sb/Fe cations are 6-coordinated [6], i.e., they are sixfold coordinated by O (48*f*) in a nearly regular octahedral geometry, with only a slight trigonal distortion. As we will see ahead, this distortion will be also reflected by the electric field gradient at the iron sites, as measured by Mössbauer spectroscopy. In this structure, the transition cations form a corner-shared tetrahedral network, as shown in Fig. 3, certainly without crystallographic order among Fe/Sb. Otherwise, extra Bragg peaks for the superstructure would be observed in the diffractograms.

Table 1 shows the parameters obtained from the Rietveld analysis for all samples prepared in the present work. The lattice parameter variation observed is consistent with the lanthanide contraction. Such agreement can also be observed on the RE–$O_{(8a)}$ bond distances (see Table 2). Also shown in this table, are the Fe/Sb–$O_{(48f)}$ distances, obtained from the Rietveld refinement of the *x* parameter, referred to 48*f* in Table 1. These distances, along with the listed angles, define the octahedral site occupied by the transition cations.

For the pyrochlores with Pr and Nd, the best refinement was obtained when A-site disorder – i.e., substitution of RE^{3+} ions by Fe^{3+} in the A-site – was considered. In both the partial substitution of the corresponding RE^{3+} ion by Fe^{3+} ion was of 16% for Pr and 11% for Nd over A-site. We are unable to propose an effective stoichiometry for any of these compounds because no evidence for substitution of iron by Pr or Nd in B-site has emerged. Also, no second phase was detected at all in these samples which makes difficult, if not impossible, to establish the real composition of these pyrochlores, in considering the mass conservation.

Actually, the occupation of A-site by small cations has been earlier investigated but, normally, in pyrochlores deliberately synthesized with excess of B cations, say, of the type $A_{2-y}B_{2+y}O_6O'$ [13,14]. Stability of some members of this family was even attributed to this disorder [14]. Such Bi-deficient pyrochlores were, eventually, found in poly-phase systems [15–17]. Another interesting feature associated with the site disorder is the displacive disorder, frequently observed through the (442) reflection in the PXRD patterns [18,15]. However, this did not appear in any of the materials studied here. For the remaining pyrochlores an improvement of the Rietveld refinements was not observed when A-site disorder was considered.

3.2. Raman analysis

Fig. 4 shows representative Raman spectra for the RE_2FeSbO_7 pyrochlore samples. The vibrational spectra of rare earth titanates [19], hafnates [20], manganates [21], and stannates [22] pyrochlores have been widely investigated. As a rule, the phonon spectra exhibit a good agreement with the group theory prevision. At the center of the Brillouin zone, the phonon distribution for the pyrochlore structure ($RE_2M_2O_7$), given by the factor group analysis, is presented in Table 3.

From the 26 vibrational normal modes of the pyrochlore structure, six modes are expected to be observed by Raman spectroscopy ($\Gamma_{Raman} = A_{1g} + E_g + 4F_{2g}$). In addition, seven modes belonging to the F_{1u} irreducible representation are infrared active. The rest of them are optically inactive (*silent*). All the Raman active

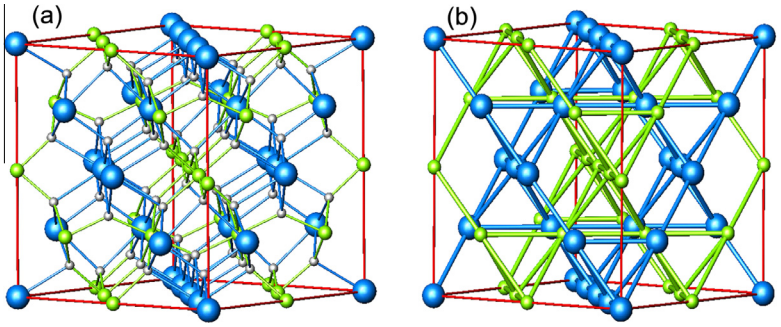

Fig. 2. Pyrochlore cubic structure for RE_2FeSbO_7: (a) red line = cell/blue spheres = RE cations (sites 16*d*)/green spheres = Fe/Sb cations (sites 16*c*)/grey little spheres = O anions; (b) detail of tetrahedral interpenetrate networks (RE ions in blue and Sb/Fe in green). (For interpretation of the references to colour in this figure legend, the reader is referred to the web version of this article.)

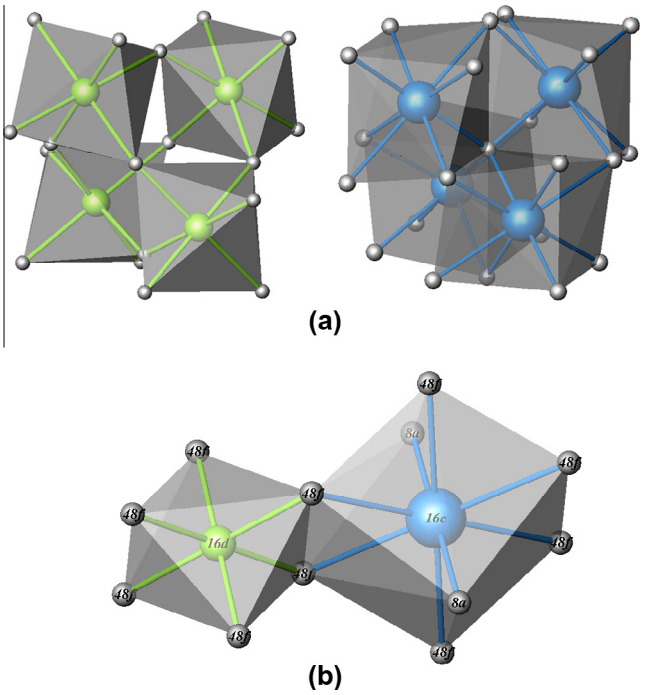

Fig. 3. (a) Tetrahedral clusters of Fe/Sb (in green) and RE (in blue); (b) oxygen polyhedra around the sites 16*c* and 16*d* and the connection between them. (For interpretation of the references to colour in this figure legend, the reader is referred to the web version of this article.)

modes are directly related to the oxygen dynamic, whereas the infrared active modes are respective to the rare earth, iron or antimony sites. According to literature data bands around 300 cm^{-1} and 520 cm^{-1} are ascribed to F_{2g}/E_g and A_{1g} irreducible representations, respectively [19,23]. There is a general agreement on the nature of the A_{1g} mode, which is related to RE–O stretching (see Fig. 5), and the overlapped modes E_g, related to the $O_{(48f)}$ sublattice, and F_{2g}, determined by O–RE–O bendings [24]. However, the complete assignment of the remaining F_{2g} modes is still subject of discussions due to their low intensity [22,25,26].

It is also worth to note that, according to calculations, none of the Raman active modes has a dominant contribution of the M–O bond stretching [27–29]. Besides the by symmetry allowed modes, the Raman spectra of most of the rare earth pyrochlores exhibit additional features due to second order-excitations, crystal field transitions and occupational disorder [23,30]. Crystal field transitions are originated in the level splitting of the RE ions, depending on their electronic configuration and local surrounding. These transitions are mainly observed at low temperatures and could contribute to the low wavenumber region of the Raman spectra [23,24,30].

Structural disorder in rare earth pyrochlores was investigated by selective cation substitution [31–33] or by applying hydrostatic pressure [34,35]. The disorder relaxes the symmetry selection rules, allowing the observation of phonons from all parts of the Brillouin zone. As a consequence, the larger number of Raman active vibrational modes could give rise to new bands and/or the broadening of those bands of the ordered structure. Some characteristic bands are usually identified at low wavenumbers (70–150 cm^{-1}), which could be attributed to the silent, acoustic or IR modes, effectively observed due to the lowering in the local symmetry originated from the lattice disorder.

For the present samples, the most intense bands of these spectra can be assigned to vibrational modes belonging to the A_{1g} (~515 cm^{-1}) and E_g/F_{2g} (~300 cm^{-1}) irreducible representations. The wide and asymmetric band identified around 750 cm^{-1} is assigned to a disordered induced two phonon process [19,23]. The observed Raman bands with the corresponding assignment, for the investigated rare earth pyrochlores are listed in Table 4. The reported assignment follows the one proposed by Maczka et al. based on single crystals polarized Raman measurements [23], as well as in far-infrared studies reported on isostructural compounds [36,37].

As stated previously, fundamental Raman active modes of the pyrochlore structure are arisen from the displacement of the two non-equivalent oxygen anions. Due to that, little dependence of the vibrational modes on the rare earth cation is observed. However, several pyrochlore families exhibit a well-established energy lowering of the A_{1g} mode on the increase of the rare earth ionic radii [22,38]. This mode was described as a distortion of the BO_6 oxygen octahedron due to a modulation of the x parameter of $O_{(48f)}$, although it may also be described as the symmetric breathing of the $O_{(48f)}$ octahedron toward the vacant site 8*b* at (3/8, 3/8, 3/8) [23,39]. According to the crystalline structure, the $O_{(48f)}$-vacancy distance is proportional to the lattice parameter ($d_{8b-48f} = a(x - 1/8)$). As a consequence, the hardening of the A_{1g} phonon can be ascribed to the lattice contraction.

On the other hand, the low wavenumber bands induced by the symmetry lowering exhibit a different behavior (see Table 4). The band observed around 80 cm^{-1} seems to be independent of the cation occupying the A site, whereas, bands around 100 and 130 cm^{-1} soften for lower rare earth ionic radii. At this point, it is worth to remember that infrared active and silent modes are not only determined by the oxygen displacements but also by the heavy cations (Table 3). Since the smaller the rare earth ionic radii the heavier the cation, phonons corresponding to the bands around 100 cm^{-1} and 130 cm^{-1} should be dominated by the

Table 1
Structure parameters, thermal isotropic parameters and some reliability factors extracted from Rietveld analysis of powder X-ray diffraction data for the RE_2SbFeO_7 compounds.

RE	Lattice parameter (A)	Wyckoff site	Fractional cell coordinates			Biso (10^{-2} A^2)	R_{bragg}	χ^2	R_{wp}
1. Pr	10.4091(1)	16*c*	0	0	0	0.85(1)	4.40	2.05	11.1
		16*d*	0.5	0.5	0.5	0.13(3)			
		48*f*	0.4211(1)	0.125	0.125	0.76(1)			
		8a	0.125	0.125	0.125	2.17(2)			
2. Nd	10.3758(1)	16*c*	0	0	0	0.75(1)	4.41	3.23	12.6
		16*d*	0.5	0.5	0.5	0.42(3)			
		48*f*	0.4196(1)	0.125	0.125	1.05(1)			
		8*a*	0.125	0.125	0.125	1.93(2)			
3. Sm	10.3401(1)	16*c*	0	0	0	0.04(2)	7.04	2.73	13.3
		16*d*	0.5	0.5	0.5	0.16(3)			
		48*f*	0.4235(2)	0.125	0.125	0.50(8)			
		8*a*	0.125	0.125	0.125	0.64(5)			
4. Eu	10.3159(2)	16*c*	0	0	0	0.32 (4)	6.39	2.61	12.9
		16*d*	0.5	0.5	0.5	0.32(3)			
		48*f*	0.4210(4)	0.125	0.125	0.28(2)			
		8*a*	0.125	0.125	0.125	0.32(4)			
5. Gd	10.2740(1)	16*c*	0	0	0	0.91(1)	5.87	3.25	14.2
		16*d*	0.5	0.5	0.5	0.66(1)			
		48*f*	0.4231(4)	0.125	0.125	1.09(2)			
		8*a*	0.125	0.125	0.125	0.02(2)			
		16*d*	0.5	0.5	0.5	0.18(3)			
		48*f*	0.4217(3)	0.125	0.125	0.47(1)			
		8*a*	0.125	0.125	0.125	0.14(5)			
6. Tb	10.2596(7)	16*c*	0	0	0	0.87(1)	3.11	3.78	18.4
		16*d*	0.5	0.5	0.5	0.18(3)			
		48*f*	0.4176(2)	0.125	0.125	1.87(3)			
		8*a*	0.125	0.125	0.125	0.79(3)			
7. Dy	10.2410(3)	16*c*	0	0	0	0.11(1)	5.87	4.58	15.0
		16*d*	0.5	0.5	0.5	0.55(1)			
		48*f*	0.4241(2)	0.125	0.125	0.30(2)			
		8*a*	0.125	0.125	0.125	0.32(2)			
8. Y	10.2081(1)	16*c*	0	0	0	0.60(1)	4.53	4.88	13.8
		16*d*	0.5	0.5	0.5	0.33(1)			
		48*f*	0.4151(3)	0.125	0.125	0.32(2)			
		8*a*	0.125	0.125	0.125	4.9(4)			
9. Ho	10.2083(1)	16*c*	0	0	0	0.63(4)	3.73	4.11	12.4
		16*d*	0.5	0.5	0.5	0.50(3)			
		48*f*	0.4202(4)	0.125	0.125	1.02(4)			
		8*a*	0.125	0.125	0.125	0.07(3)			
10. Er	10.1992(1)	16*c*	0	0	0	0.29(2)	6.47	4.90	12.1
		16*d*	0.5	0.5	0.5	0.18(3)			
		48*f*	0.4217(3)	0.125	0.125	0.47(1)			
		8*a*	0.125	0.125	0.125	0.14(5)			
11. Yb	10.1635(1)	16*c*	0	0	0	0.35(1)	5.69	6.00	13.2
		16*d*	0.5	0.5	0.5	0.24(2)			
		48*f*	0.4224(4)	0.125	0.125	2.24(1)			
		8*a*	0.125	0.125	0.125	0.06(2)			

oscillation of the atom at the 16*c* site because phonon energy is inversely proportional to the mass of the rare earth. On the other hand, the low energy band ($\sim$80 cm^{-1}) should be associated to the 16*d* site since the same cations are place at this site in all the investigated samples.

3.3. Mössbauer spectroscopy

Fig. 6 shows the Mössbauer spectra for the same samples of Fig. 1. The hyperfine parameters fitted for these and all other RE_2FeSbO_7 compounds are listed in Table 5. As it can be seen, the spectrum for the Nd_2FeSbO_7 sample (as well as for the Pr_2FeSbO_7 sample) was fitted with two doublets, whereas for the spectra of all other samples only one doublet was enough in accomplishing good fits. In every case, the isomer shifts are typical of trivalent iron. Earlier studies conducted by others on the iron-antimony pyrochlores, measured at RT, reported just one subspectral component for all RE's [9]. The fitted hyperfine parameters – δ and Δ – obtained in the present investigation are in relative agreement with previously reported values. Higher velocity Mössbauer spectra were also taken (not shown), in order to verify the presence of magnetic components which, finally, were not observed.

It is also worthy of saying that samples with the same nominal chemical composition, prepared by similar synthesis routes, can present some fine structural differences, as revealed by the Mössbauer spectra. After some repetitions in preparing determined samples, we observed that for some RE's a second iron site can eventually be observed, even when a monophasic sample – as evidenced by XRD – was obtained. The experience showed us that the larger is the ionic radius more probable is the appearance of that second site for iron in the Mössbauer pattern of the sample. Reflecting this trend, we could not prepare the Pr_2SbFeO_7 and Nd_2SbFeO_7 pyrochlores without a second doublet (i.e., the largest one) in their Mössbauer spectra, even after many synthesis tries, at different heat treatment temperatures. We attribute this second subspectrum to iron cations occupying the RE site (16*c*), in the

Table 2
Some distances and angles between oxygen and metal cations in RE_2SbFeO_7, as refined from Rietveld method.

Pyrochlore	RE–$O_{(8a)}$ RE–$O_{(48f)}$ distances (Å)	Fe/Sb–$O_{(48f)}$ distances (Å)	(Fe/Sb)–O–(Fe/Sb) angle (°)	O–(Fe/Sb)–O angle (°)
Pr_2FeSbO_7	2 × 2.2536(2) 6 × 2.5606(6)	6 × 2.0152(6)	131.88(2)	83.71(6) 96.29(3)
Nd_2FeSbO_7	2 × 2.2464(1) 6 × 2.5419(8)	6 × 2.0150(7)	131.09(2)	83.19(7) 96.81(3)
Sm_2FeSbO_7	2 × 2.2387(3) 6 × 2.5613(6)	6 × 1.9917(5)	133.20(2)	84.59(5) 95.41(2)
Eu_2FeSbO_7	2 × 2.2335(4) 6 × 2.5368(3)	6 × 1.9976(3)	131.81(1)	83.67(3) 96.34(1)
Gd_2FeSbO_7	2 × 2.2244(1) 6 × 2.5419(3)	6 × 1.9806(3)	132.98(1)	84.44(3) 95.56(1)
Tb_2FeSbO_7	2 × 2.2213(2) 6 × 2.4992(8)	6 × 2.0010(8)	130.02(2)	82.49(7) 97.51(3)
Dy_2FeSbO_7	2 × 2.2173(4) 6 × 2.5411(3)	6 × 1.9701(3)	133.54(1)	84.81(3) 95.19(1)
Y_2FeSbO_7	2 × 2.2101(2) 6 × 2.4694(3)	6 × 2.0017(3)	128.71(1)	81.64(2) 98.36(1)
Ho_2FeSbO_7	2 × 2.2102(2) 6 × 2.5050(3)	6 × 1.9800(3)	131.40(1)	83.39(2) 96.61(1)
Er_2FeSbO_7	2 × 2.2082(2) 6 × 2.5131(3)	6 × 1.9721(3)	132.19(1)	83.92(3) 96.08(1)
Yb_2FeSbO_7	2 × 2.2005(2) 6 × 2.5098(4)	6 × 1.9621(3)	132.61(1)	84.19(3) 95.81(1)

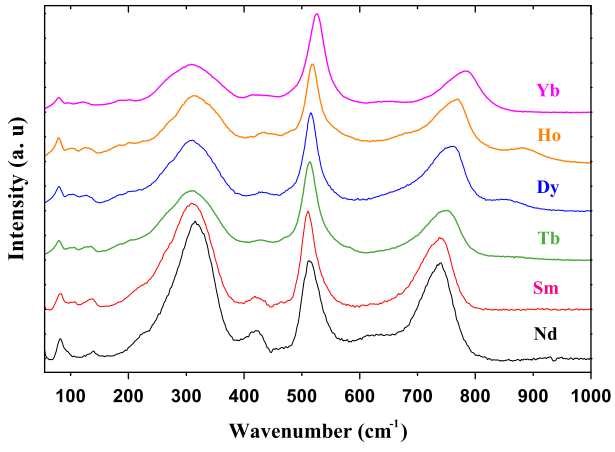

Fig. 4. Raman spectra for the RE_2FeSbO_7 samples.

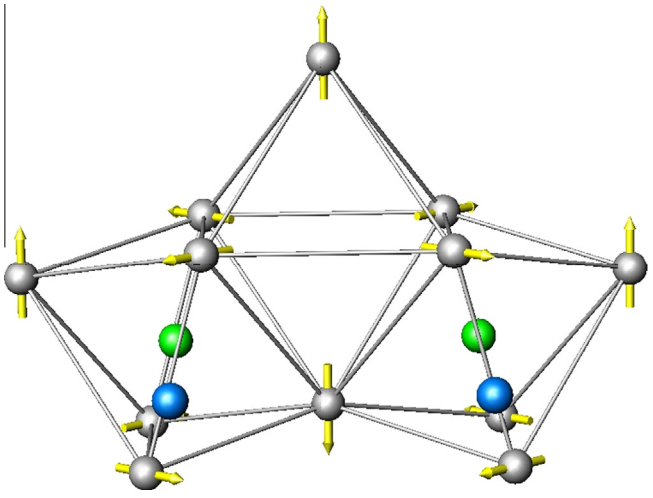

Fig. 5. Schematic representation of the A_{1g} Raman excitation.

Table 3
Factor analysis for the RE_2SbFeO_7 samples.

Atoms	Sites	Symmetry	Irreducible representations
RE	16*c*	−3*m*	$A_{2u} + E_u + F_{1u} + F_{2u}$
Sb/Fe	16*d*	−3*m*	$A_{2u} + E_u + F_{1u} + F_{2u}$
O_1	48*f*	2*mm*	$A_{1g} + A_{2u} + E_u + E_g + 3F_{1u} + 2F_{1g} + 2F_{2u} + 3F_{2g}$
O_2	8*a*	−43*m*	$F_{1u} + F_{2g}$

$\Gamma_{TOTAL} = A_{1g} + E_g + 2F_{1g} + 4F_{2g} + 3A_{2u} + 3E_u + 8F_{1u} + 4F_{2u}$; $\Gamma_{ACOUSTIC} = F_{1u}$; $\Gamma_{INFRARED} = 7\ F_{1u}$; $\Gamma_{RAMAN} = A_{1g} + E_g + 4F_{2g}$.

same way it was observed for Bi_2FeMO_7 (M = Ta and Sb) pyrochlores [18]. Throughout some unknown mechanism, larger ionic radii (i.e., 0.99 Å, 0.983 Å and 1.03 Å, for Pr^{3+}, Nd^{3+} and Bi^{3+}, respectively) favor the occupancy of site 16*c* by Fe^{3+} cations. This is consistent with the improvement shown by the Rietveld refinements for these pyrochlores, in which an A-site disorder was taken into account.

Table 4
Raman bands (cm^{-1}) for the RE_2SbFeO_7 pyrochlores.

Nd	Sm	Tb	Dy	Ho	Yb	Assignment
82	82	80	79	79	79	Phonon (IR)
	104	102	103	102	97	Phonon (IR)
137	134	130	128	127	120	Phonon (IR)
		182	178	181	186	Phonon
221	219	203	206	202	203	F_{2g}
316	310	311	311	316	307	E_g/F_{2g}
419	421	430	430	434	434	F_{2g}
511	511	513	516	518	525	A_{1g}/F_{2g}
624	704	686	686	678	651	Second order
718	728	741	741	751	757	Second order
745	749	767	767	773	789	Second order
		860	860	885		Second order

The A-site disorder determined by Mössbauer spectroscopy (see Table 5) is a little lower than the obtained by the refinement of the PXRD data. However, it is meaningful how both measurement

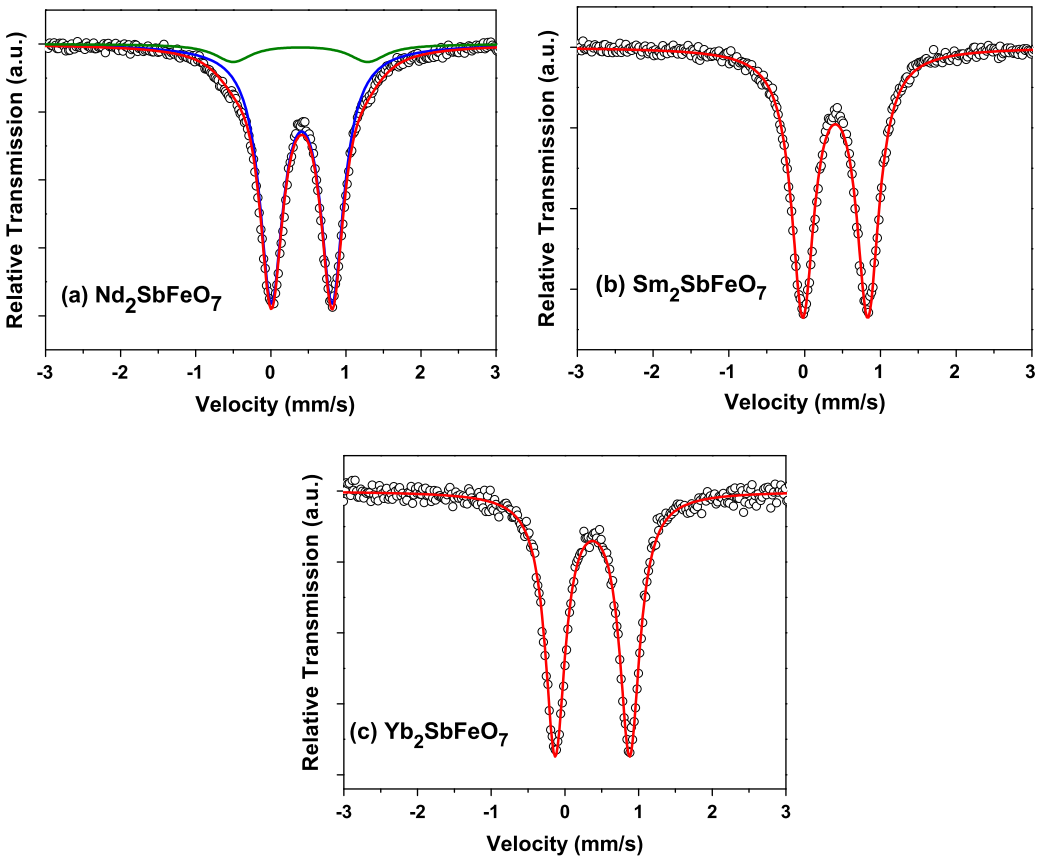

Fig. 6. Mössbauer spectra for the Nd_2FeSbO_7 (a), Sm_2FeSbO_7 (b) and Yb_2FeSbO_7 (c) samples.

Table 5
Hyperfine parameters for the RE_2FeSbO_7 compounds. (δ = *Isomer shift;* Δ = *quadrupole splitting;* Γ = *linewidth*).

Pyrochlore	δ[a] (mm/s)	Δ (mm/s)	Γ (mm/s)	Site area (%)
1. Pr_2FeSbO_7	0.41	0.77	0.37	89
	0.33	1.90	0.55	11
2. Nd_2FeSbO_7	0.41	0.81	0.37	91
	0.39	1.80	0.60	9
3. Sm_2FeSbO_7	0.40	0.85	0.35	100
4. Eu_2FeSbO_7	0.40	0.88	0.35	100
5. Gd_2FeSbO_7	0.39	0.91	0.37	100
6. Tb_2FeSbO_7	0.39	0.93	0.34	100
7. Dy_2FeSbO_7	0.38	0.97	0.32	100
8. Y_2FeSbO_7	0.38	1.00	0.37	100
9. Ho_2FeSbO_7	0.38	1.01	0.33	100
10. Er_2FeSbO_7	0.38	1.03	0.32	100
11. Yb_2FeSbO_7	0.37	1.05	0.33	100

[a] Relative to α-Fe at RT.

techniques agree in revealing such A-site disorder. The presence of some silent, acoustic or IR modes, effectively observed in Raman spectra for this family of pyrochlores, due to the lowering in the local symmetry originated from the lattice disorder, can be addressed to the presence of A-site disorder as well, even for the remaining samples, where such disorder can be quite small and it is not evident from PXRD data.

Fig. 7 displays the lattice parameter, the A_{1g} wavenumber, the quadrupole splitting and the d_{RE-O}, all as functions of the RE (trivalent and 8-coordinated) ionic radius for the RE_2FeSbO_7 compounds. First of all, we see that there is a linear variation of the two geometric attributes drawn in the graphics, the lattice parameter and the RE–O distance, with the RE ionic radius. In addition, it can be distinguished a correlation between A_{1g} with RE^{3+}–$O_{(8a)}$, evidencing the relation of this Raman mode to the RE–O stretching.

Finally, as pointed out earlier, the A_{1g} Raman mode is primarily related to the distortion of the BO_6 oxygen octahedron, or, alternatively, as the symmetric breathing of the $O_{(48f)}$ octahedron toward the vacant site 8*b*. However, in this family of pyrochlores such correlation is not observed, and this is because the octahedral

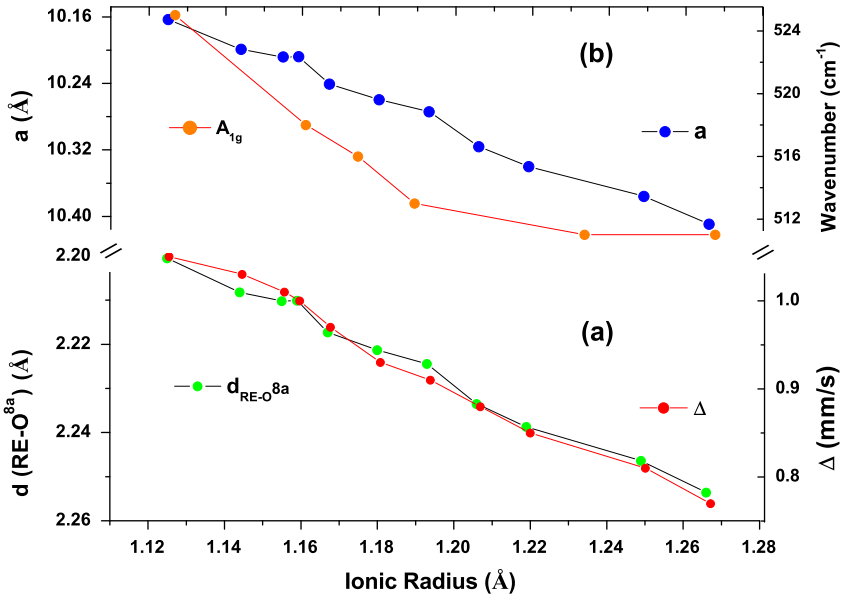

Fig. 7. Lattice parameter (blue balls/left axis) and A_{1g} wavenumber (orange balls/right axis) – upper – quadrupole splitting (red balls/right axis) and d_{RE-O} (green balls/left axis) – (lower) –, all as a function of the RE ionic radius, for the RE_2FeSbO_7 compounds. (For interpretation of the references to colour in this figure legend, the reader is referred to the web version of this article.)

environment, around 8*a* and 8*b* sites, remains almost symmetric with the substitution of RE^{3+} ions.

It can be also verified that Δ increases as *a* decreases (see Fig. 7a). This demonstrates that the lanthanide contraction implies an increase of the distortion from the cubic symmetry at the iron sites. Such distortion, although finely dependent on the oxygen positions (48*f*), surprisingly seems not to be directly related to an inner octahedral distortion. Apparently, the BO_6 octahedron are enough regular: they show a gradually decreasing $B–O_{(48f)}$ distances and the internal distortion – see $O–Fe^{3+}/Sb^{5+}–O$ angles in Table 2 – do not follow any tendency inside the polyhedron. By another side, the bigger is the ionic radius of the RE^{3+} ion, the lower is the distortion of the second coordination sphere around the iron ion, whereas the octahedron remains almost invariant. Thus, the observed correlation between Δ and lattice parameter is apparently more related to the second coordination sphere of O^{2-} ions, as clearly shown in Fig. 7b.

4. Conclusions

The RE_2FeSbO_7 pyrochlores, with RE = Pr, Nd, Sm, Eu, Gd, Tb, Dy, Y, Ho, Er and Yb, crystallize with the *Fd*-3*m* symmetry, with iron/antimony cations statistically distributed over the site 16*c* of the cubic pyrochlore structure. Iron cations tend to occupy also the 16*d* site for the light RE. The lattice parameter of these compounds increases linearly with the RE ionic radius, whereas the distortion from the cubic symmetry of the 16*c* site increases with decreasing ionic radius. The distortion of the iron site seems to be more related to the distortion of the oxygen polyhedra in the second coordination sphere than the distortion of the octahedral formed by the nearest oxygens.

References

[1] J.E. Greedan, Review: frustrated rare earth magnetism: spin glasses, spin liquids and spin ices in pyrochlore oxides, J. Alloys Comp. 408–412 (2006) 444–455.
[2] A.P. Ramirez, in: K.J.H. Buschow (Ed.), Handbook of Magnetic Materials, vol. 13, Elsevier, Amsterdam, 2001, pp. 423–520.
[3] J.S. Gardner, M.J.P. Gingras, J.E. Greedan, Magnetic pyrochlore oxides, Rev. Mod. Phys. 82 (2010) 53–107.
[4] N.P. Raju, E. Gmelin, R.K. Kremer, Magnetic-susceptibility and specific-heat studies of spin-glass-like ordering in the pyrochlore compounds $R_2Mo_2O_7$ (R = Y, Sm, or Gd), Phys. Rev. B 46 (1992) 5405–5411.
[5] G. Chen, H. Takenoshita, H. Satoh, N. Kamegashira, M. Miyamoto, Structural analysis of complex oxides $Ln_2MnTa_{1+x}O_{7+\alpha}$ (Ln = Rare Earth and Yttrium) with pyrochlore-related structures, J. Alloys Comp. 374 (2004) 177–180.
[6] M.A. Subramanian, G. Aravamudan, G.V. Subba Rao, Oxide pyrochlores – review, Prog. Solid State Chem. 15 (2) (1983) 55–141.
[7] C.K. Matsuda, F.F. Ivashita, A. Paesano Jr., E.V. Pannunzio Miner, M.C. Blanco, R.E. Carbonio, J.B. Marimon da Cunha, L. Ghivelder, Structural, Structural, hyperfine and magnetic properties of RE_2FeTaO_7 compounds (RE = Y, Dy, Gd and Eu), Phys. Rev. B 81 (2010) 014417.
[8] M.C. Montmory, E.F. Bertaut, Étude de quelques composés de terres rares isotypes du pyrochlore, C.R. Acad. Sci. 252 (1961) 4171 (Paris).
[9] O. Knop, F. Brisse, R.E. Meads, J. Bainbridge, Pyrochlores IV: crystallographic and Mössbauer studies of A_2FeSbO_7 pyrochlores, Can. J. Chem. 46 (1968) 3829–3832.
[10] C.K. Matsuda, R. Barco, P. Sharma, V. Biondo, A. Paesano Jr., J.B.M. da Cunha, B. Hallouche, Iron-containing pyrochlores: structural and magnetic characterization, Hyperfine Interact. 175 (2007) 55–61.
[11] G. Filoti, M. Rosenberg, V. Kuncser, B. Seling, T. Fries, A. Spies, S. Kemmler, Sack, magnetic properties and cation distribution in iron containing pyrochlores, J. Alloys Comp. 268 (1998) 16–21.
[12] J. Rodríguez-Carvajal, Physica B 192 (1993) 55–59.
[13] B. Melot, E. Rodriguez, Th. Proffen, M.A. Hayward, R. Seshadri, Displacive disorder in three high-k bismuth oxide pyrochlores, Mater. Res. Bull. 41 (2006) 961–966.
[14] T.A. Vanderah, I. Levin, M.W. Lufaso, An unexpected crystal-chemical principle for the pyrochlore structure, Eur. J. Inorg. Chem. (2005) 2895–2901.
[15] M.W. Lufaso, T.A. Vanderah, I.M. Pazos, I. Levin, R.S. Roth, J.C. Nino, V. Provenzano, P.K. Schenck, Phase formation, crystal chemistry, and properties in the system $Bi_2O_3–Fe_2O_3–Nb_2O_5$, J. Solid State Chem. 179 (2006) 3900–3910.
[16] R.S. Roth, T.A. Vanderah, P. Bordet, I.E. Grey, W.G. Mumme, L. Cai, J.C. Nino, Pyrochlore formation, phase relations, and properties in the $CaO–TiO_2–(Nb, Ta)_2O_5$ systems, J. Solid State Chem. 181 (2008) 406–414.
[17] W. Miiller, L. Causeret, C.D. Ling, Frustrated magnetism, Frustrated magnetism and local structural disorder in pyrochlore-type $Bi_{1.89}Fe_{1.16}Nb_{0.95}O_{6.95}$, J. Phys.: Condens. Matter 22 (2010) 1–7.
[18] M.C. Blanco, D.G. Franco, Y. Jalit, E.V. Pannuzio Miner, G. Berndt, A. Paesano, G. Nieva, R.E. Carbonio, Synthesis, magnetic properties and Mössbauer spectroscopy for the pyrochlore family $Bi_2BB'O_7$ with B = Cr and Fe and B′ = Nb, Ta and Sb, Phys. B: Condens. Matter 407 (2012) 3078–3080.
[19] M. Maczka, J. Hanuza, K. Hermanowicz, A.F. Fuentes, K. Matsuhira, Z. Hiroi, Temperature-dependent Raman scattering studies of the geometrically frustrated pyrochlores $Dy_2Ti_2O_7$, $Gd_2Ti_2O_7$ and $Er_2Ti_2O_7$, J. Raman Spectrosc. 39 (4) (2008) 537–544.
[20] H.C. Gupta, S. Brown, N. Rani, A lattice dynamical investigation of the Raman and the infrared frequencies of the cubic $A_2Hf_2O_7$ pyrochlores, J. Phys. Chem. 63 (2002) 2–5.
[21] S. Brown, H.C. Gupta, J.A. Alonso, M.J. Martinez-Lope, Vibrational spectra and force field calculation of $A_2Mn_2O_7$ (A = Y, Dy, Er, Yb) pyrochlores, J. Raman Spectrosc. 34 (3) (2003) 240–243.

[22] M.T. Vandenborre, E. Husson, J.P. Chatry, D. Michel, Rare-earth titanates and stannates of pyrochlore structure; vibrational spectra and force fields, J. Raman Spectrosc. 14 (2) (1983) 63–71.
[23] M. Maczka, M. Sanjuán, A. Fuentes, L. Macalik, J. Hanuza, K. Matsuhira, Z. Hiroi, Temperature-dependent studies of the geometrically frustrated pyrochlores $Ho_2Ti_2O_7$ and $Dy_2Ti_2O_7$, Phys. Rev. B 79 (21) (2009) 214437.
[24] T. Lummen, I. Handayani, M. Donker, D. Fausti, G. Dhalenne, P. Berthet, A. Revcolevschi, P.H.M. van Loosdrecht, Phonon and crystal field excitations in geometrically frustrated rare earth titanates, Phys. Rev. B 77 (21) (2008) 214310.
[25] S. Saha, D. Muthu, C. Pascanut, N. Dragoe, R. Suryanarayanan, G. Dhalenne, A. Revcolevschi, S. Karmakar, S.M. Sharma, A.K. Sood, High-pressure Raman and X-ray study of the spin-frustrated pyrochlore $Gd_2Ti_2O_7$, Phys. Rev. B 74 (6) (2006) 064109.
[26] F.X. Zhang, B. Manoun, S.K. Saxena, C.S. Zha, Structure change of pyrochlore $Sm_2Ti_2O_7$ at high pressures, Appl. Phys. Lett. 86 (18) (2005) 181906.
[27] S. Brown, H.C. Gupta, J. Alonso, M. Martínez-Lope, Lattice dynamical study of optical modes in $Tl_2Mn_2O_7$ and $In_2Mn_2O_7$ pyrochlores, Phys. Rev. B 69 (5) (2004) 054434.
[28] H.C. Gupta, S. Brown, N. Rani, V.B. Gohel, Lattice dynamic investigation of the zone center wavenumbers of the cubic $A_2Ti_2O_7$ pyrochlores, J. Raman Spectrosc. 32 (1) (2001) 41–44.
[29] M. Sanjuán, C. Guglieri, S. Díaz-Moreno, G. Aquilanti, A. Fuentes, L. Olivi, J. Chaboy, Raman and X-ray absorption spectroscopy study of the phase evolution induced by mechanical milling and thermal treatments in $R_2Ti_2O_7$ pyrochlores, Phys. Rev. B 84 (10) (2011) 104207.
[30] S. Saha, S. Prusty, S. Singh, R. Suryanarayanan, A. Revcolevschi, A.K. Sood, Pyrochlore "dynamic spin-ice" $Pr_2Sn_2O_7$ and monoclinic $Pr_2Ti_2O_7$: a comparative temperature-dependent Raman study, J. Solid State Chem. 184 (8) (2011) 2204–2208.
[31] M. Lang, J. Lian, J. Zhang, F. Zhang, W. Weber, C. Trautmann, R. Ewing, Single-ion tracks in $Gd_2Zr_{2-x}Ti_xO_7$ pyrochlores irradiated with swift heavy ions, Phys. Rev. B 79 (22) (2009) 224105.
[32] F.N. Sayed, V. Grover, K. Bhattacharyya, D. Jain, A. Arya, C.G.S. Pillai, A.K. Tyagi, $Sm_{2-x}Dy_xZr_2O_7$ pyrochlores: probing order-disorder dynamics and multifunctionality, Inorg. Chem. 50 (6) (2011) 2354–2365.
[33] C. Wan, Z. Qu, A. Du, W. Pan, Order-disorder transition and unconventional thermal conductivities of the $(Sm_{1-x}Yb_x)_2Zr_2O_7$ series, J. Am. Ceram. Soc. 94 (2) (2011) 592–596.
[34] A.K. Mishra, H.K. Poswal, S.M. Sharma, S. Saha, D.V.S. Muthu, S. Singh, R. Suryanarayanan, A. Revcolevschi, A.K. Sood, The study of pressure induced structural phase transition in spin-frustrated $Yb_2Ti_2O_7$ pyrochlore, J. Appl. Phys. 111 (3) (2012) 033509.
[35] F. Zhang, M. Lang, Z. Liu, R. Ewing, Pressure-induced disordering and anomalous lattice expansion in $La_2Zr_2O_7$ pyrochlore, Phys. Rev. Lett. 105 (1) (2010) 015503.
[36] C.Z. Bi, J.Y. Ma, B.R. Zhao, Z. Tang, D. Yin, C.Z. Li, D.Z. Yao, J. Shi, X.G. Qiu, Far infrared optical properties of the pyrochlore spin ice compound $Dy_2Ti_2O_7$, J. Phys.: Condens. Matter 17 (34) (2005) 5225–5233.
[37] Z. Qi, X. Cheng, B. Liu, G. Zhang, Y. Chen, C. Li, M. Yin, Vibrational and dielectric properties of $La_2Hf_2O_7$: experiment and theory, Solid State Commun. 151 (18) (2011) 1288–1292.
[38] T.T. Zhang, K.W. Li, J. Zeng, Y.L. Wang, X.M. Song, H. Wang, Synthesis and structural characterization of a series of lanthanide stannate pyrochlores, J. Phys. Chem. Sol. 69 (11) (2008) 2845–2851.
[39] T. Hasegawa, Y. Takasu, N. Ogita, M. Udagawa, J. Yamaura, Y. Nagao, Z. Hiroi, Raman scattering in KOs_2O_6, Phys. Rev. B 77 (6) (2008) 064303.